SCIENCE CHINA
Chemistry

• ARTICLES •
· SPECIAL ISSUE · Dedicated to the 60th Anniversary of Institute of Chemistry, CAS

October 2016 Vol.59 No.10: 1270–1276
doi: 10.1007/s11426-016-0105-8

Unraveling weak interactions in aniline-pyrrole dimer clusters

Chengqian Yuan[1,2], Pan An[1], Jing Chen[1], Zhixun Luo[1*] & Jiannian Yao[1*]

[1]*Beijing National Laboratory for Molecular Sciences, Institute of Chemistry, Chinese Academy of Sciences, Beijing 100190, China*
[2]*Graduate University of Chinese Academy of Sciences, Beijing 100049, China*

Received March 10, 2016; accepted April 20, 2016; published online July 25, 2016

Weak intermolecular interactions in aniline-pyrrole dimer clusters have been studied by the dispersion-corrected density functional theory (DFT) calculations. Two distinct types of hydrogen bonds are demonstrated with optimized geometric structures and largest interaction energy moduli. Comprehensive spectroscopic analysis is also addressed revealing the orientation-dependent interactions by noting the altered red-shifts of the infrared and Raman activities. Then we employ natural bond orbital (NBO) analysis and atom in molecules (AIM) theory to have determined the origin and relative energetic contributions of the weak interactions in these systems. NBO and AIM calculations confirm the V-shaped dimer cluster is dominated by N−H···N and C−H···π hydrogen bonds, while the J-aggregated isomer is stabilized by N−H···π, n→π* and weak π···π* stacking interactions. The noncovalent interactions are also demonstrated via energy decomposition analysis associated with electrostatic and dispersion contributions.

weak intermolecular interactions, aniline, pyrrole, dimer cluster, hydrogen bonding, nature bond orbital, energy decomposition

Citation: Yuan C, An P, Chen J, Luo Z, Yao J. Unraveling weak interactions in aniline-pyrrole dimer clusters. *Sci China Chem*, 2016, 59: 1270–1276, doi: 10.1007/s11426-016-0105-8

1 Introduction

Weak intermolecular interactions, such as hydrogen bonding and π···π* stacking, are ubiquitous in many areas of science and engineering ranging from chemistry [1,2], biology [3] to materials science [4]. Accordingly, they have attracted reasonable research interest to scientists working in such fields as to tune material properties and to understand biological functions, etc. In general, complex processes including the self-assembly of nanomaterials, reproduction of biological information stored in DNA, and even some chemical reactions are governed by a subtle balance among various weak noncovalent interactions. How these interactions mutually influence each other is a question of interest [5], and this has been the target of intense experimental and theoretical efforts.

Among the multitude noncovalent interactions, traditional N−H···N hydrogen bonding and amino-aromatic (i.e. N−H···π) interactions are crucial binding forces in both chemical and biological systems [6–8]. Recent years have witnessed a substantial number of studies to such individual weak interactions. Knowledge on the manifestation of intermolecular interactions and their relative preferences is crucial in rational design of materials with desired properties. To acquire a clear understanding on this, a few molecular cluster systems have been studied via theoretical or experimental approaches [9–13]. For example, two different types of hydrogen bonding interactions have been observed between the amino group in aniline and aromatic rings of furan, toluene, and benzene, etc.

*Corresponding authors (email: zxluo@iccas.ac.cn; jnyao@iccas.ac.cn)

Aniline, the simplest amine with an aromatic ring, is an important precursor for chemical syntheses. Meanwhile, pyrrole is a significant aromatic heterocyclic broadly used in material science and found in naturally occurring and biologically important molecules [14,15]. Keeping this in mind, we have selected aniline-pyrrole dimer clusters as the prototypical model, in view of the possible coexistence of N–H···π and N–H···N bound conformers. In addition, the pK_a value of aniline is positive and the NH_2 part can act as a weak base, while that of pyrrole is negative and the NH part may act as a weak acid. The positive/negative pK_a values of aniline and pyrrole enable a stable dimer cluster via strong hydrogen binding interaction. We have investigated the structures, interaction energies, and vibrational frequencies using various density functional theory (DFT) calculations. The natural bond orbital (NBO) and atom in molecules (AIM) theory analyses, and generalized Kohn-Sham based energy decomposition analysis (GKS-EDA) are also carried out to study the nature of the weak interactions stabilizing aniline-pyrrole dimer clusters. The molecular-level understanding of these weak interactions is beneficial for designing synthetic proteins and advanced functional materials.

2 Computational methods

All the quantum chemical calculations were carried out within the Gaussian 09 program package [16] with the default convergence criteria without any constraint on the geometry. Geometries were optimized and binding energies evaluated by using various basis sets in conjunction with the dispersion-corrected DFT M06-2X, and ωB97X-D levels of theory. Multiple structures of possible aniline-pyrrole dimer cluster conformers used as initial geometries for optimization were provided in Scheme 1. The harmonic vibrational frequencies calculation on the optimized geometries were performed at each level of theory, which ensures the structures as minima and enable the evaluation of zero-point vibrational energies (ZPVE). The vibrational frequency calculations confirmed that all optimized dimer clusters have no imaginary frequencies and are stable structures. Interaction energies were defined as the difference between the energy of the dimer cluster and the sum of the monomers, in their optimized geometries, and were corrected for ZPVE and basis set superposition error (BSSE) via the counterpoise procedure [17]. Quantitative assessments of charge transfer between individual orbitals were made via the NBO method [18], as implemented in the Gaussian 09 software. AIM analyses were performed with the Multifunctional Wavefunction Analyzer (Multiwfn) software [19] at the ωB97X-D/6–311++G(d,p) level. Decomposition of the interaction energies was achieved using the GKS-EDA method [20] at the ωB97X-D/6-311++g(d,p) level in help of Dr. Su. The GKS-EDA scheme divides the total interaction energy into six terms:

$$\Delta E_{int} = \Delta E_{ele} + \Delta E_{ex} + \Delta E_{rep} + \Delta E_{pol} + \Delta E_{corr} + \Delta E_{disp} \quad (1)$$

where ΔE_{ele} is the electrostatic interaction energy, calculated from monomers' Kohn-Sham orbitals. ΔE_{ex} and ΔE_{rep} denote the exchange and repulsion interaction respectively, arising from the anti-symmetrization and normalization of Kohn-Sham determinants. The sum of ΔE_{ex} and ΔE_{rep} is also known as Pauli repulsion. ΔE_{pol} represents the polarization interaction due to the variation of Kohn-Sham orbitals by self-consistent field (SCF) procedure; ΔE_{corr} stands for the correlation interaction defined by the GKS correlation energy; ΔE_{disp} is the dispersion interaction which is optional for dispersion correction DFT.

3 Results and discussion

Several structures of the aniline-pyrrole dimer clusters have been modeled for geometry optimization at different levels of dispersion corrected DFT using various basis sets. To facilitate the discussion below, the structures stabilized by N–H···N and N–H···π hydrogen bonding are named as HB and PD respectively. It is interesting to find that all the initial structures are converged to the three types of structures after geometry optimization (as shown in Figure S1, Supporting Information online). BSSE and ZPVE corrected interaction energies of the obtained stable structures of the dimer

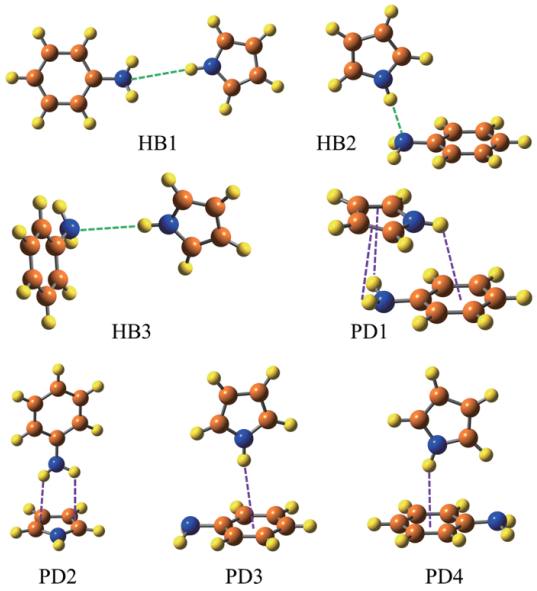

Scheme 1 Structures of possible conformers for the aniline-pyrrole dimer cluster. These structures are used as initial geometries for optimization. The green and purple lines denote the N–H···N and N–H···π hydrogen bonds respectively (color online).

clusters calculated at corresponding level of theory are provided in Table 1. It is noteworthy that the order of the interaction energies of different structures calculated at all levels of theory has a similar trend. These results indicate that the most stable HB and PD structures of the aniline-pyrrole dimer cluster are anpy1 and anpy2, respectively. Figure 1 depicts the optimized structures of anpy1 and anpy2 calculated at the ωB97X-D/6-311++g(d,p) level of theory, where the HB structure gets a unique V-shaped geometry to maximize the stability through additional C−H···π interactions and the PD structure mainly stabilized by N−H···π interactions exhibits a J-aggregated geometry. Atom numbering scheme in the dimer clusters has also been shown in Figure 1.

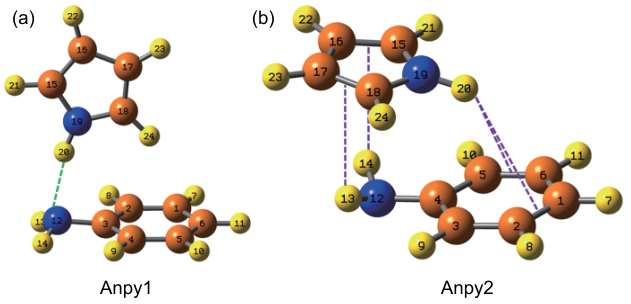

Figure 1 The optimized structures of aniline-pyrrole dimer clusters mainly stabilized by (a) N−H···N hydrogen bonding, and (b) N−H···π interaction. The green and purple lines denote the N−H···N and N−H···π hydrogen bonds respectively (color online).

A few selected intermolecular geometrical parameters including the H···Y distance (R), bond length variations of X–H bonds (ΔR), and the bond angles of X–H···Y are also displayed in Table 2. One typical manifestation of hydrogen bond is its effect upon the X–H covalent bond of the proton donor molecule, which indicates how strongly the X–H group is involved in the hydrogen bonding interaction. Generally, majority of X–H bonds are elongated via the formation of the traditional hydrogen bonds. The shorter H···Y bond or the longer X–H bond is, the stronger the interaction is, and vice versa [21,22]. The ΔR data for the conventional N–H···N and unconventional N–H···π, C–H···π hydrogen bonds in Table 2 are all positive, indicating stretching behaviour of such bonds. In addition, the ΔR values for the N–H···N bonding is larger than that for N–H···π and C–H···π interactions, however, the distance between H···Y exhibits a converse trend. These data reveal that the average N–H···N hydrogen bonding interaction is stronger than the average N–H···π and C–H···π interactions in aniline-pyrrole dimer cluster structures.

Fingerprints of structural spectroscopy provide a powerful technique for characterizing the hydrogen bonding interactions [23]. In view of this, we have calculated infrared activities of aniline-pyrrole dimer clusters by comparing with those of the corresponding monomers. Of interest here are the vibrational frequencies of the NH and CH stretch modes, which are primarily affected by dimer cluster formation. Figure 2 presents the theoretical IR spectra of the monomers

Table 1 BSSE and ZPVE corrected interaction energies (kcal/mol) of aniline-pyrrole dimer clusters calculated at various levels of DFT

Theory	Aniline-pyrrole dimer cluster					
	anpy1		anpy2		anpy3	
	ΔE_e [a]	ΔE_0 [b]	ΔE_e	ΔE_0	ΔE_e	ΔE_0
ωB97X-D/6-311++g(d,p)	–7.76	–6.54	–8.24	–6.73	–6.63	–5.90
ωB97X-D/6-311++g(2d,p)	–7.57	–6.17	–8.09	–6.83	–6.65	–5.81
ωB97X-D/6-311++g(3d,p)	–7.53	–6.16	–7.97	–6.73	–6.59	–5.78
ωB97X-D/6-311++g(2d,2p)	–7.46	–6.09	–7.91	–6.81	–6.52	–5.66
ωB97X-D/aug-cc-pvdz	–7.44	–6.32	–7.95	–7.02	–6.44	–5.78
M06-2X/6-311++g(d,p)	–7.18	–5.95	–8.18	–7.18	–6.27	–5.52

a) ΔE_e: BSSE corrected interaction energy; b) ΔE_0: BSSE+ZPE corrected interaction energy.

Table 2 Geometric parameters (bond length and angle) and stretching vibrational frequencies (cm^{-1}) of hydrogen bond in aniline-pyrrole dimer cluster calculated at the ωB97X-D/6-311++G(d,p) level of theory

Dimer cluster	X–H···Y	ΔR (Å) [a]	R (Å) [b]	∠X–H···Y (°)	$\Delta\nu$ [c]
anpy1	N19–H20···N12	0.0089	2.1260	163.2	–146
	C18–H24···C1–C6	0.0010	2.9993	156.6	–7
	C18–H24···C4–C5	0.0010	2.9527	133.9	–7
anpy2	N19–H20···C1–C2	0.0026	3.2006	136.7	–32
	N19–H20... C1–C2	0.0026	3.0379	116.1	–32
	N12–H13···C17–C18	0.0022	2.9563	112.8	–13 (–25)
	N12–H14···C15–C16	0.0022	2.9405	113.1	–13 (–25)

a) ΔR denotes the bond length variations of X–H bonds before and after dimer cluster formation; b) R represents the distance between the hydrogen atom, covalently attached to the carbon or nitrogen atom, and the nitrogen atom or centroid of the C=C bond; c) $\Delta\nu$=ν(dimer cluster)–ν (free monomer), the numbers in the parentheses refer to the $\Delta\nu$ values of antisymmetric stretching modes.

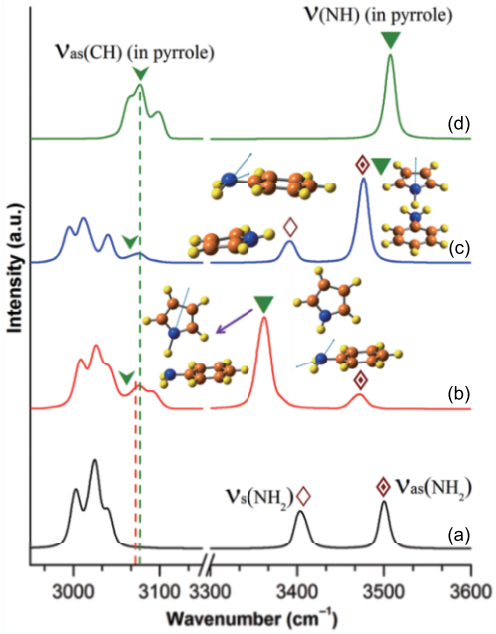

Figure 2 The IR spectra of (a) aniline monomer, (b) anpy1 dimer cluster, (c) anpy2 dimer cluster, and (d) pyrrole monomer (color online).

and dimer clusters in the mentioned region calculated at the ωB97X-D/6-311++g(d,p) level of theory. As shown in Figure 2(a), two absorption bands centered at ~3404 and 3501 cm^{-1} are assigned to the NH_2 symmetric and antisymmetric stretching vibrations of aniline (marked by purple and wine arrow respectively). The NH stretching vibration of pyrrole is observed at ~3508 cm^{-1} in Figure 2(d) (labeled by green triangle). It is notable that the IR spectra of the aniline-pyrrole dimer clusters are quite different from that of monomers rather than the linear superposition of them. Specially, the bands observed at around 3362 and 3472 cm^{-1} in the spectrum of anpy1 (Figure 2(b)) belong to the NH stretching vibration of pyrrole and antisymmetric stretching vibration of aniline, which leads to a red shift of 146 and 29 cm^{-1} compared to those found for the free pyrrole and aniline monomer respectively. With respect to anpy2, the intense peak appearing at 3476 cm^{-1} is ascribe to the NH antisymmetric stretching of aniline and stretching mode of pyrrole, as well as a weak band at ~3391 cm^{-1} assigned to the NH symmetric stretching vibration of aniline. Such assignment gives rise to red shifts of 13 cm^{-1} for NH symmetric stretching mode and 25 cm^{-1} for antisymmetric stretching vibration compared to those observed for the free aniline monomer, which are close to those observed in the aniline dimer cluster and the aniline-benzene complexes, indicating a similar interaction between the NH_2 group and the pyrrole π system [11,24]. Besides, we select the strongest CH antisymmetric stretching mode at ~3077 cm^{-1} (marked by green rhomb) in pyrrole to probe whether a certain interaction is contributed by the CH group. A comparison study on the IR spectra of pyrrole, anpy1, and anpy2 reveals a slightly red-shift in anpy1, which confirms the existence of weak C–H···π interactions in anpy1. The red shifts of the X–H stretching vibrational mode have been traditionally considered as one of the main fingerprints of hydrogen bonds, assuming that formation of a hydrogen bond weakens the X–H single bond. The larger the shift value is, the stronger the H bond is. Therefore, N–H···N interaction is stronger than the N–H···π and C–H···π interactions.

Raman activity (Figure 3) is also calculated to further examine the weak interactions of the aniline-pyrrole dimer clusters. A clear and minor red-shift of the C–H symmetric stretching mode is also noted in the Raman spectra of anpy1, verifying the existence of weak intermolecular interactions (e.g. C–H···π interactions). In addition, the red-shift features of the N–H stretching are discovered again in the aniline-pyrrole dimer clusters, further confirming the existence of intermolecular interactions (e.g. N–H···N and N–H···π interactions). No surprise that the Raman and IR spectra have provided complementary information regarding the dimer cluster structures and weak intermolecular interactions.

According to the early reports, the red-shifted hydrogen bonds are mainly attributed to two aspects [22]. On one hand, the electrostatic attraction between the higher electronegativity Y and the positive H elongates the X–H bond. On the other hand, the charge-transfer or hyperconjugative interaction between the proton donor and the proton acceptor weakens and lengthens the X–H bond, hence leading to red shift of the X–H stretching mode.

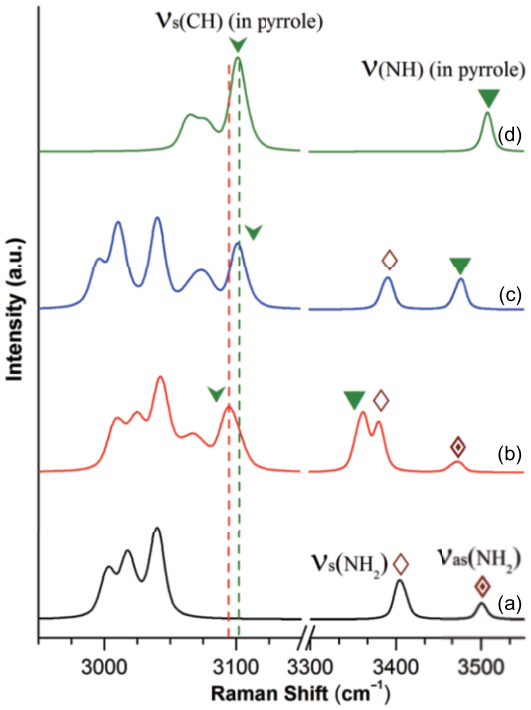

Figure 3 The Raman spectra of (a) aniline monomer, (b) anpy1 dimer cluster, (c) anpy2 dimer cluster, and (d) pyrrole monomer (color online).

To explore the interaction origin and determine the strength of the interactions involved in the dimer clusters, NBO analyses have been performed. With regard to traditional hydrogen bonding interaction, the charge transfer delocalization occurs between the lone pair orbital of the hydrogen bond acceptor (N atom) and the antibonding orbital of the hydrogen bond donor (N–H group). On the other hand, the unconventional hydrogen bond interaction including N–H···π as well as C–H···π interaction is achieved through the delocalization of the π-orbitals of the hydrogen bond acceptor over the antibonding orbital of the hydrogen bond donor. Figure 4 displays the NBOs showing the overlap between the N atom lone pair orbitals or π-orbitals and antibonding orbitals of the N–H or C–H groups. The NBO delocalization energy used for estimating the energy decrease caused by the electron delocalization in hydrogen bonding interaction is determined by the second-order perturbative energy, $E^{(2)}_{i\to j*}$, where i and j^* stand for an acceptor and a donor orbital, respectively. Total $E^{(2)}_{i\to j*}$ values for anpy1 and anpy2 are 8.69 and 1.98 kcal/mol, respectively. It is worth mentioning that the binding in anpy2 is stronger than that in anpy1, in contrast to the result of NBO calculation which is mainly based on the charge transfer interaction. Such calculation results reinforce that anpy1 is dominantly stabilized by charge-transfer hydrogen bonding, while anpy2 is governed by dispersion-dominant weak interactions, allowing anpy2 to possess the stronger binding but with a lower $E^{(2)}_{i\to j*}$.

The details of NBO analysis for the aniline-pyrrole dimer clusters are listed in Table 3, where the individual N–H···N interaction is found much stronger than the individual N–H···π and C–H···π interaction. The most important finding is that the appearance of n→π* interaction in anpy2 arises from the delocalization of the N atom lone pair orbitals over the antibonding π-orbitals. This interaction is widely present in biomolecules and materials [3,25], which has been observed by probing the IR-UV double-resonance spectroscopy in a supersonic jet [26]. In addition, a few pairs of π···π* stacking interactions are observed in anpy2 dimer cluster, which is helpful for decreasing the dimer cluster energy furtherly hence resulting in an improved structure stability. Moreover, a couple of π···π* stacking backward interactions is observed in anpy2, as depicted in Figure S2. Therefore, the NBO analysis is in favor of the aforementioned conclusion from the structure and vibrational frequencies analyses.

We have tried to use AIM analyses to further the intermolecular interactions of aniline-pyrrole dimer clusters. According to Bader's AIM methodology, the values of the electron density (ρ) and its Laplacian ($\nabla^2\rho$) at their BCPs give valuable information about the strength and type of a bond [27]. Specifically, ρ is used to describe the strength of a bond,

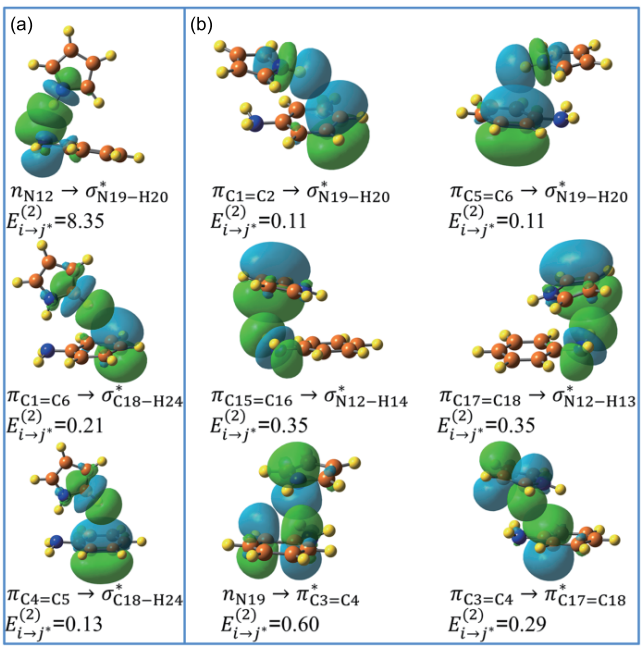

Figure 4 Natural bond orbitals in the aniline-pyrrole dimer clusters showing (a) N–H···N and C–H···π hydrogen bonding, and (b) N–H···π, n→π* and π···π* interactions. All the second-order perturbative energy is in kcal/mol (color online).

Table 3 NBO analysis of the intermolecular weak interactions in the aniline-pyrrole dimer clusters calculated at the ωB97X-D/6-311++g(d,p) level of theory. The second-order perturbation energies $E^{(2)}_{i\to j*}$ are in kcal/mol

Dimer cluster	Donor	Acceptor	$E^{(2)}_{i\to j*}$	Sum of $E^{(2)}_{i\to j*}$
anpy1	LP (1) N12	BD*(1) N19–H20	8.35	8.69
	BD (2) C1–C6	BD*(1) C18–H24	0.21	
	BD (2) C4–C5	BD*(1) C18–H24	0.13	
anpy2	BD (2) C1–C2	BD*(1) N19–H20	0.11	1.98
	BD (2) C5–C6	BD*(1) N19–H20	0.11	
	BD (2) C15–C16	BD*(1) N12–H14	0.35	
	BD (2) C17–C18	BD*(1) N12–H13	0.35	
	LP (1) N19	BD*(2) C3–C4	0.60	
	BD (2) C3–C4	BD*(2) C17–C18	0.29	
	BD (2) C5–C6	BD*(2) C15–C16	0.07	
	BD (2) C15–C16	BD*(2) C5–C6	0.10	

Table 4 Selected topological parameters of the bond critical point (BCP) in the aniline-pyrrole dimer clusters calculated at the ωB97X-D/6-311++g(d,p) level of theory

Dimer cluster	BP	ρ	$\nabla^2\rho$	H
anpy1	H20···N12	0.020457	0.064657	0.001833
	H24···C1–C6	0.005544	0.018042	0.000776
anpy2	H13···C18	0.006109	0.017609	0.000565
	H14···C15	0.006112	0.017614	0.000566
	N19···C4	0.008979	0.030212	0.0011147

and the larger ρ value means a stronger bond; $\nabla^2\rho$ is used to characterize the bond, where negative $\nabla^2\rho$ means the interatomic bond exists as a covalent bond, while positive $\nabla^2\rho$ values suggest ionic bonds, hydrogen bonds, or van der Waals interactions. In view of this, three most fundamental criteria for the existence of hydrogen bond are indicated, that is, there exists a BCP, and the values of ρ and its $\nabla^2\rho$ bear ranges at 0.002–0.035 and 0.024–0.139 a.u. respectively. In addition, if the total electron energy densities at critical point (H) are positive, the nature of the interaction is purely noncovalent. Table 4 list some typical topological parameters of BCPs involved in the interactions of aniline-pyrrole dimer clusters. It is noted that all the $\nabla^2\rho$ and H values are positive, proving the existence of weak noncovalent interactions in the aniline-pyrrole dimer clusters. It is evident that the ρ and $\nabla^2\rho$ values at BCP between the H20 and N12 atoms are within the aforementioned range, verifying the existence of N19–H20··· N12 traditional hydrogen bond in anpy1 dimer cluster. With respect to the X–H···π interactions, the ρ values are all within the scope of decisive criteria, while the $\nabla^2\rho$ values are beyond the lower-limit of the range. Therefore, X–H···π interactions function as weak hydrogen bonding. Regarding to the N19···C4 interaction, the higher ρ value compared to those of X–H···π interactions indicates n→π^* interaction is strong than the individual X–H··· π interaction.

Continuing to explore the nature of above mentioned noncovalent interactions contributing to the stabilization of the aniline-pyrrole dimer clusters, we have tried GKS-EDA analysis in help of Dr. Su [20]. It is verified that electrostatic interaction is the largest contribution for the total interaction of anpy1, while the correlation interaction and dispersion dominate the total interaction energy of anpy2. Also anpy1 dimer cluster falls into the category of the electrostatic dominated hydrogen bonded dimer cluster, but anpy2 dimer cluster stabilized by four nonconventional N–H···π hydrogen bonds as well as n→π^* interactions in addition to π···π^* stacking caters for the scope of "special mixed-influence" (SMI) dimer clusters [28,29]. Moreover, the relatively large polarization energy in anpy1 suggests that the N–H orbitals in pyrrole undergo significant changes in their shapes in order to maximize the strength of the hydrogen bond during the dimer cluster formation process [30]. It is also noted that the sum of correlation interaction and dispersion interaction in anpy2 is larger than that in anpy1, largely due to the presence of unconventional π–H bonding and dispersion dominated n→π^* and π··· π^* stacking interactions in anpy2 dimer cluster. These results are consistent with the aforementioned NBO analysis.

4 Conclusions

In summary, we have investigated the weak intermolecular interactions in aniline-pyrrole molecular dimer clusters employing the dispersion-corrected DFT calculations. A stable N−H···N hydrogen bond dimer cluster and an unconventional N−H···π hydrogen bond dimer cluster are predicted through the DFT calculations using various levels of theory, and a comparison of interaction energies demonstrates that the latter dimer cluster is more stable than the former. Comprehensive infrared and Raman vibrational frequency analysis for the two dimer clusters reveals that remarkable interactions by noting the large red-shifts of the modes corresponding to hydrogen bond. Furtherly, we employed NBO and AIM analyses to have determined the origin and relative energetic contributions of the weak interactions in these systems. These results reveal that the V-shaped dimer cluster is held by N−H··· N hydrogen bond and C−H···π interaction, while the tilted parallel displaced dimer cluster is stabilized by N−H···π as well as n→π^* and π···π^* stacking interactions simultaneously. Energy decomposition analysis of the interactions energy indicates that electrostatics interactions dominantly contribute to the stability of anpy1 dimer cluster. The present work provides insights into an in-depth understanding at the molecular level of the amino-aromatic interactions involved in some complex chemical and biological process.

Acknowledgments We thank Professor P.F. Su in Xiamen University for GKS-EDA analysis and friendly discussion of the results. This work was supported by the National Project "Development of Advanced Scientific Instruments Based on Deep Ultraviolet Laser Source" (Y31M0112C1) and the National Basic Research Program of China (2011CB808402). Z. Luo acknowledges the Young Professionals Programme in Institute of Chemistry, Chinese Academy of Sciences (ICCAS-Y3297B1261).

Conflict of interest The authors declare that they have no conflict of interest.

Supporting information The supporting information is available online

at http://chem.scichina.com and http://link.springer.com/journal/11426. The supporting materials are published as submitted, without typesetting or editing. The responsibility for scientific accuracy and content remains entirely with the authors.

1 Cho Y, Cho WJ, Youn IS, Lee G, Singh NJ, Kim KS. *Acc Chem Res*, 2014, 47: 3321–3330
2 Bouteiller L, van der Schoot P. *J Am Chem Soc*, 2012, 134: 1363–1366
3 Bartlett GJ, Newberry RW, VanVeller B, Raines RT, Woolfson DN. *J Am Chem Soc*, 2013, 135: 18682–18688
4 Wei P, Yan X, Huang F. *Chem Soc Rev*, 2015, 44: 815–832
5 Saha S, Sastry GN. *J Phys Chem B*, 2015, 119: 11121–11135
6 Scheiner S, Kar T, Pattanayak J. *J Am Chem Soc*, 2002, 124: 13257–13264
7 Paytakov G, Dinadayalane T, Leszczynski J. *J Phys Chem A*, 2015, 119: 1190–1200
8 Fornaro T, Biczysko M, Monti S, Barone V. *Phys Chem Chem Phys*, 2014, 16: 10112–10128
9 Nakanaga T, Ito F. *J Phys Chem A*, 1999, 103: 5440–5445
10 Piracha NK, Ito F, Nakanaga T. *Chem Phys*, 2004, 297: 133–138
11 Ohashi K, Inokuchi Y, Izutsu H, Hino K, Yamamoto N, Nishi N, Sekiya H. *Chem Phys Lett*, 2000, 323: 43–48
12 Kawamata K, Chowdhury PK, Ito F, Sugawara K, Nakanaga T. *J Phys Chem A*, 1998, 102: 4788–4793
13 Liu Y, Liu W, Li H, Liu J, Yang Y. *J Phys Chem A*, 2006, 110: 11760–11764
14 Stefov V, Pejov L, Šoptrajanov B. *J Mol Struct*, 2003, 651–653: 793–805
15 Gómez-Zavaglia A, Fausto R. *J Phys Chem A*, 2004, 108: 6953–6967
16 Frisch M, Trucks G, Schlegel HB, et al. Gaussian 09. Secondary. Wallingford CT: Gaussian, Inc., 2009
17 Boys SF, Bernardi FD. *Mol Phys*, 1970, 19: 553–566
18 Weinhold F, Landis CR. *Valency and Bonding: A Natural Bond Orbital Donor-Acceptor Perspective.* Cambridge: Cambridge University Press, 2005
19 Lu T, Chen F. *J Comput Chem*, 2012, 33: 580–592
20 Su P, Jiang Z, Chen Z, Wu W. *J Phys Chem A*, 2014, 118: 2531–2542
21 Niu X, Huang Z, Ma L, Shen T, Guo L. *J Chem Sci*, 2013, 125: 949–958
22 Zhou PP, Qiu WY. *J Phys Chem A*, 2009, 113: 10306–10320
23 Mondal SI, Dey A, Sen S, Patwari GN, Ghosh D. *Phys Chem Chem Phys*, 2015, 17: 434–443
24 Schemmel D, Schütz M. *J Chem Phys*, 2010, 132: 174303
25 Singh SK, Das A. *Phys Chem Chem Phys*, 2015, 17: 9596–9612
26 Singh SK, Mishra KK, Sharma N, Das A. *Angew Chem Int Ed*, 2016, 55: 7801–7805
27 Bader RFW. *Atoms in Molecules.* Place Published: John Wiley & Sons Ltd, 1990
28 Jurečka P, Šponer J, Černý J, Hobza P. *Phys Chem Chem Phys*, 2006, 8: 1985–1993
29 Řezáč J, Riley KE, Hobza P. *J Chem Theor Comput*, 2011, 7: 3466–3470
30 Su P, Li H. *J Chem Phys*, 2009, 131: 014102